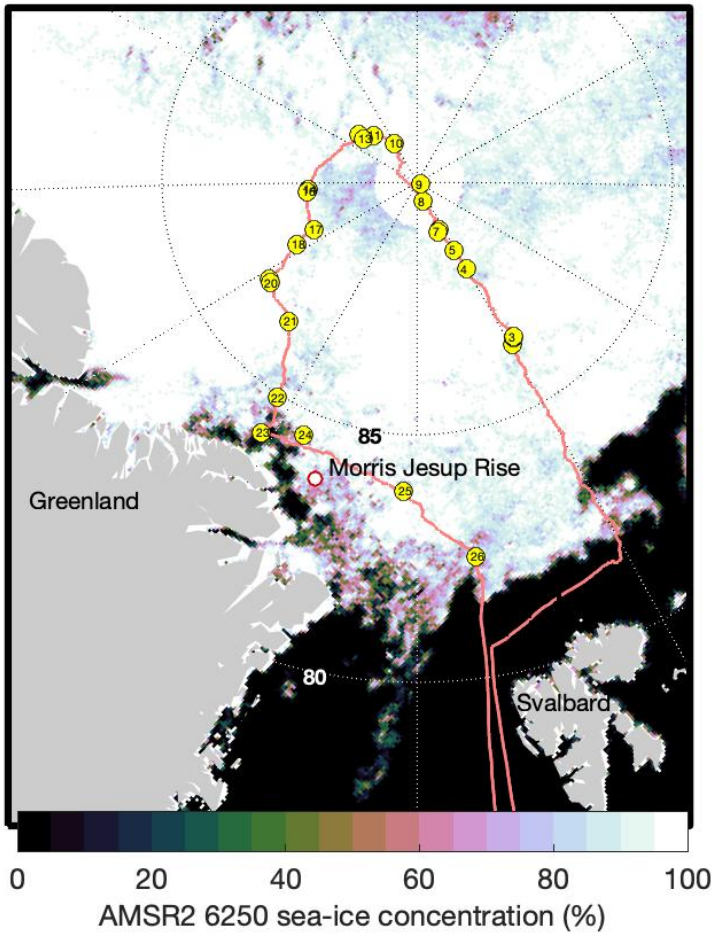

Figure 1. Map of the expedition route (red line) with chamber flux sampling locations (yellow circles) and numbers corresponding to Table S1. Sea-ice concentration is shown as determined for 2021-9-1 by AMSR-2 satellite observations and the ASI 6.25km^2 product.

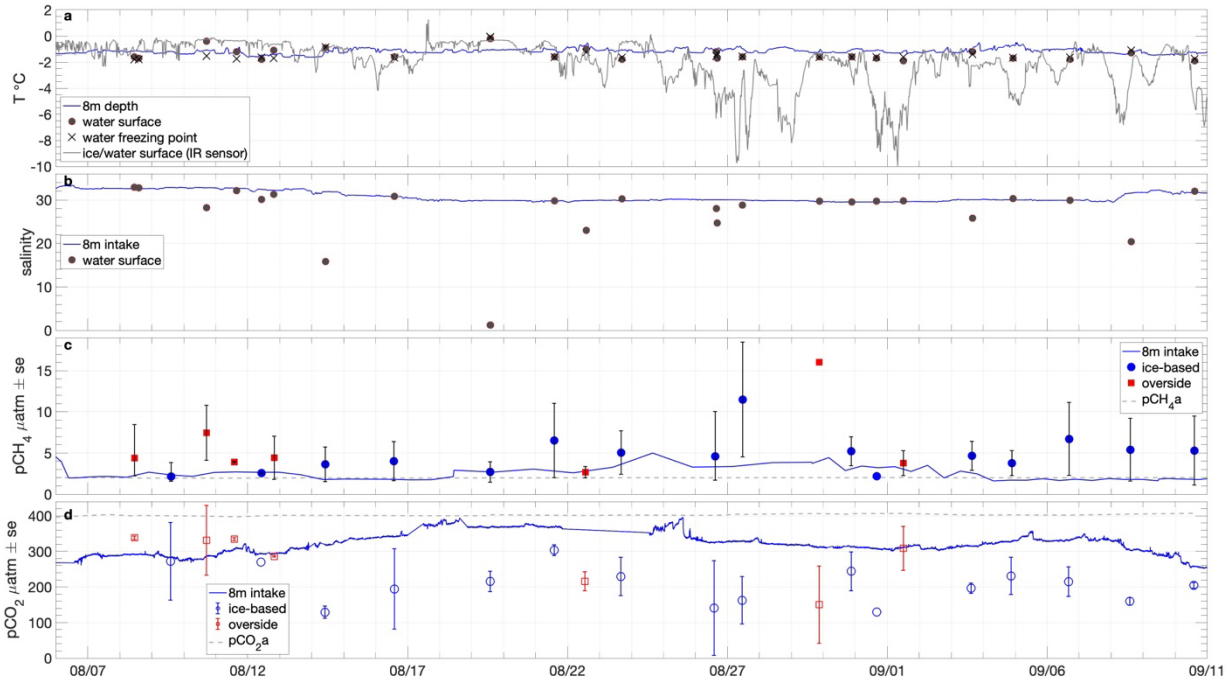

Figure 4. Time series of: a) seawater temperature at 8m depth and at the surface during chamber flux sampling, the corresponding freezing point determined from salinity measurement, and surface temperature (ice or water) measured from IR sensors onboard *Oden*; b) Salinity measured from the 8 m intake and at the surface during chamber flux sampling; c) partial pressures of CH_4 in water at specified depths and sampling locations and in the near-surface atmosphere; d) as per c for CO_2.

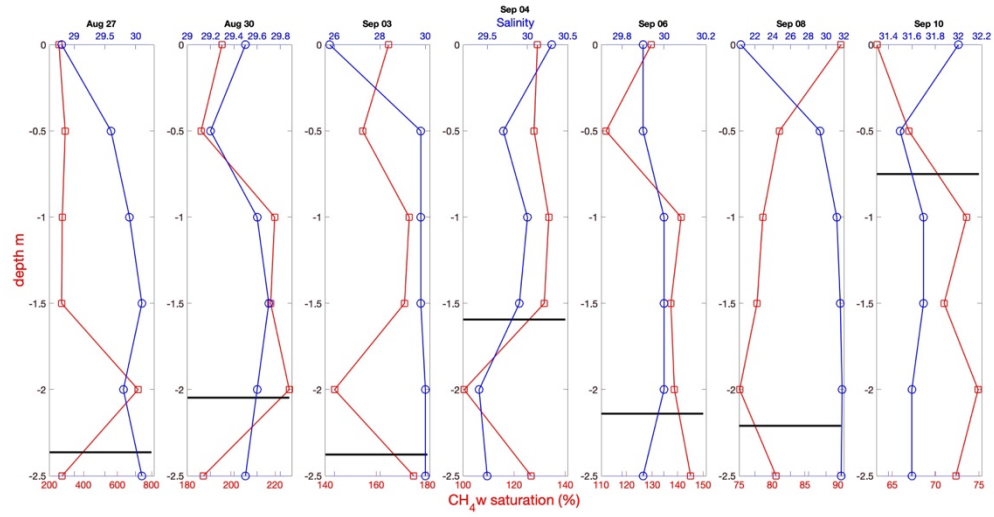

Figure 5. Near-surface profiles of CH_4 saturation (red) and salinity (blue) determined from ice-based Ruttner bottle sampling on the indicated day. An estimate of ice floe thickness is shown (thick black line), determined from auger drilling close to the sampling site.

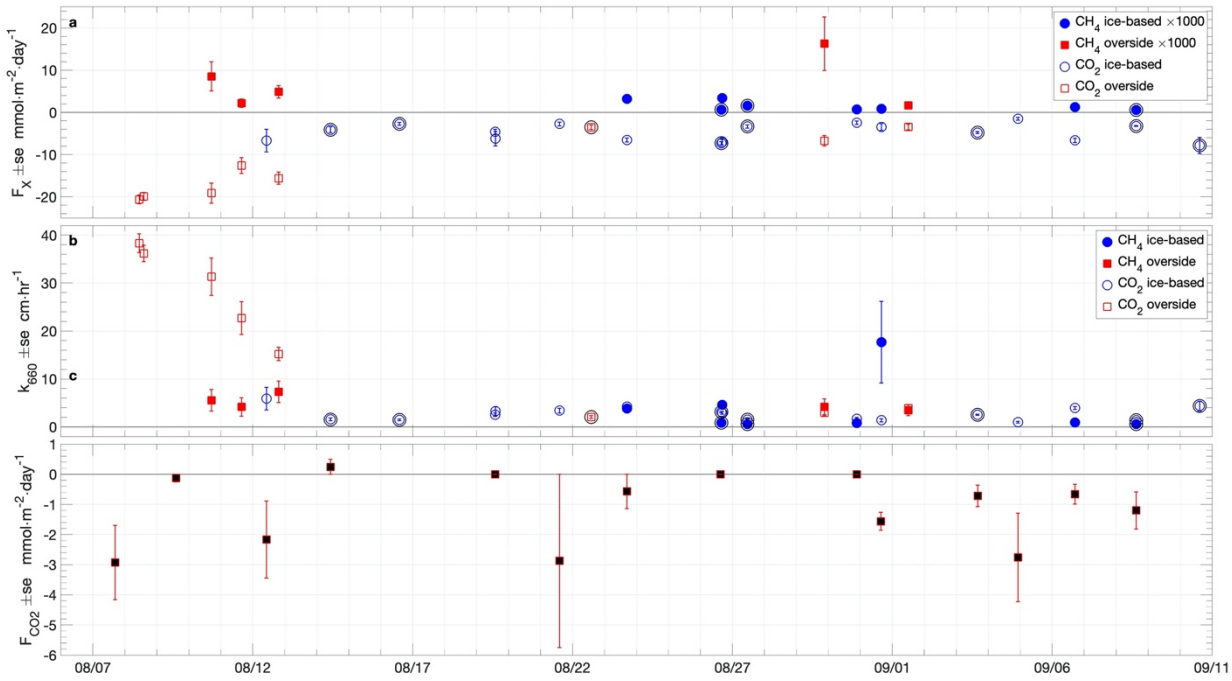

Figure 6. Time series of: a) air-sea fluxes of CH_4 (filled symbols) and CO_2 (non-filled symbols) measured with chamber flux systems at the specified sampling locations; b) k_{660} of CH_4 (filled symbols) and CO_2 (non-filled symbols) determined from air-sea chamber flux measurements using equations 1 and 2; c) snow-air CO_2 fluxes measured with the EGM-4 chamber flux system. Error bars are the standard error of the flux samples in each deployment. Outer black circles in a and b indicate measurements made in the presence of grease ice.

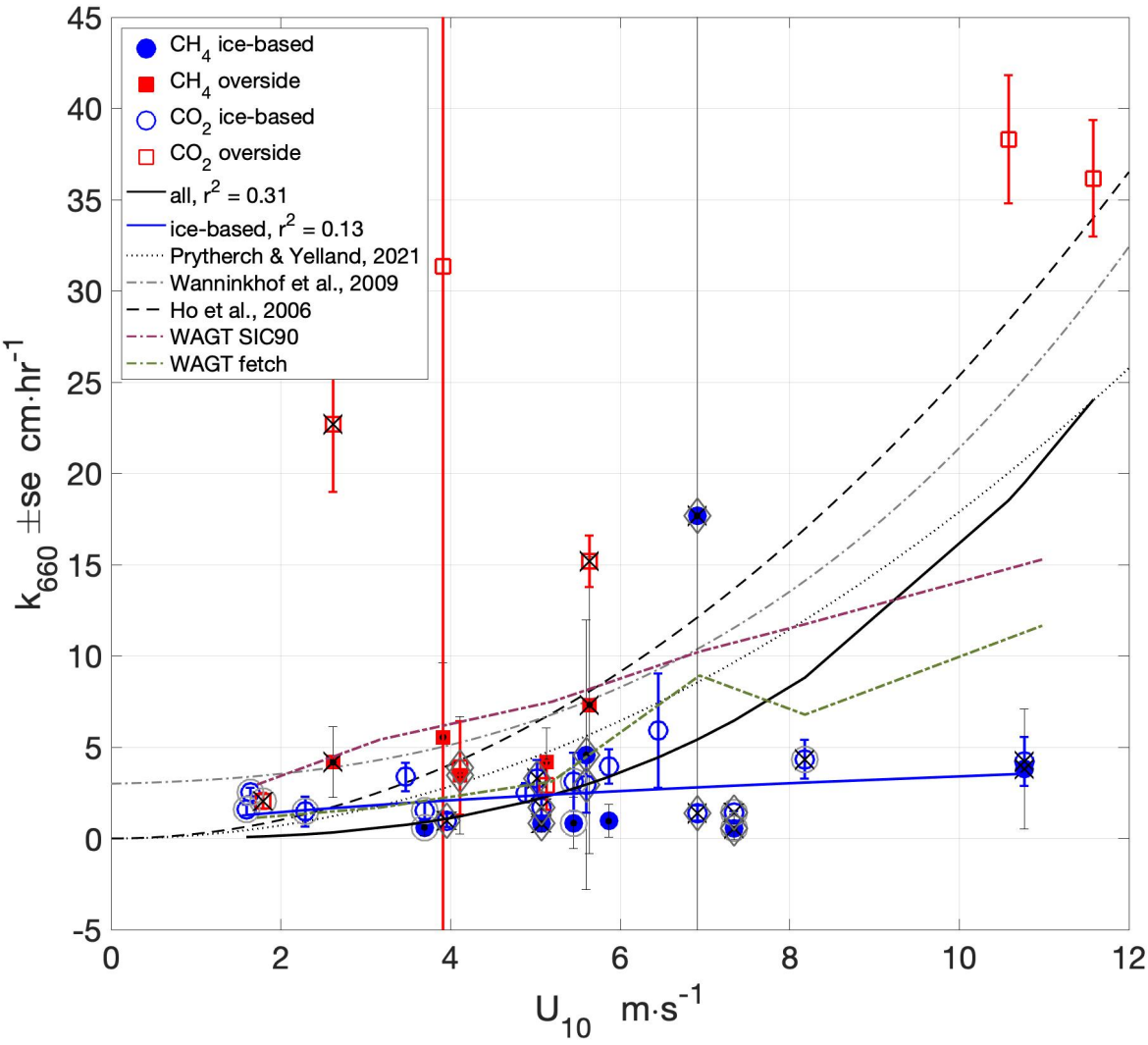

Figure 7. Wind speed dependence of k_{660} determined from air-sea chamber flux measurements using Eqs. (1) and (2), and non-linear least squares fits to the measurements ($y = a \times x^b$). Outer circles around the markers indicate measurements made in the presence of grease ice. Black crosses indicate measurements made with lead widths < 10 m. Diamonds indicate measurements made when surface buoyancy flux was negative (surface cooling). Also shown are three wind speed-based parameterisations of k_{660}. And the parametric WAGT model in both SIC mode (with SIC = 90%) and fetch mode using lead width.

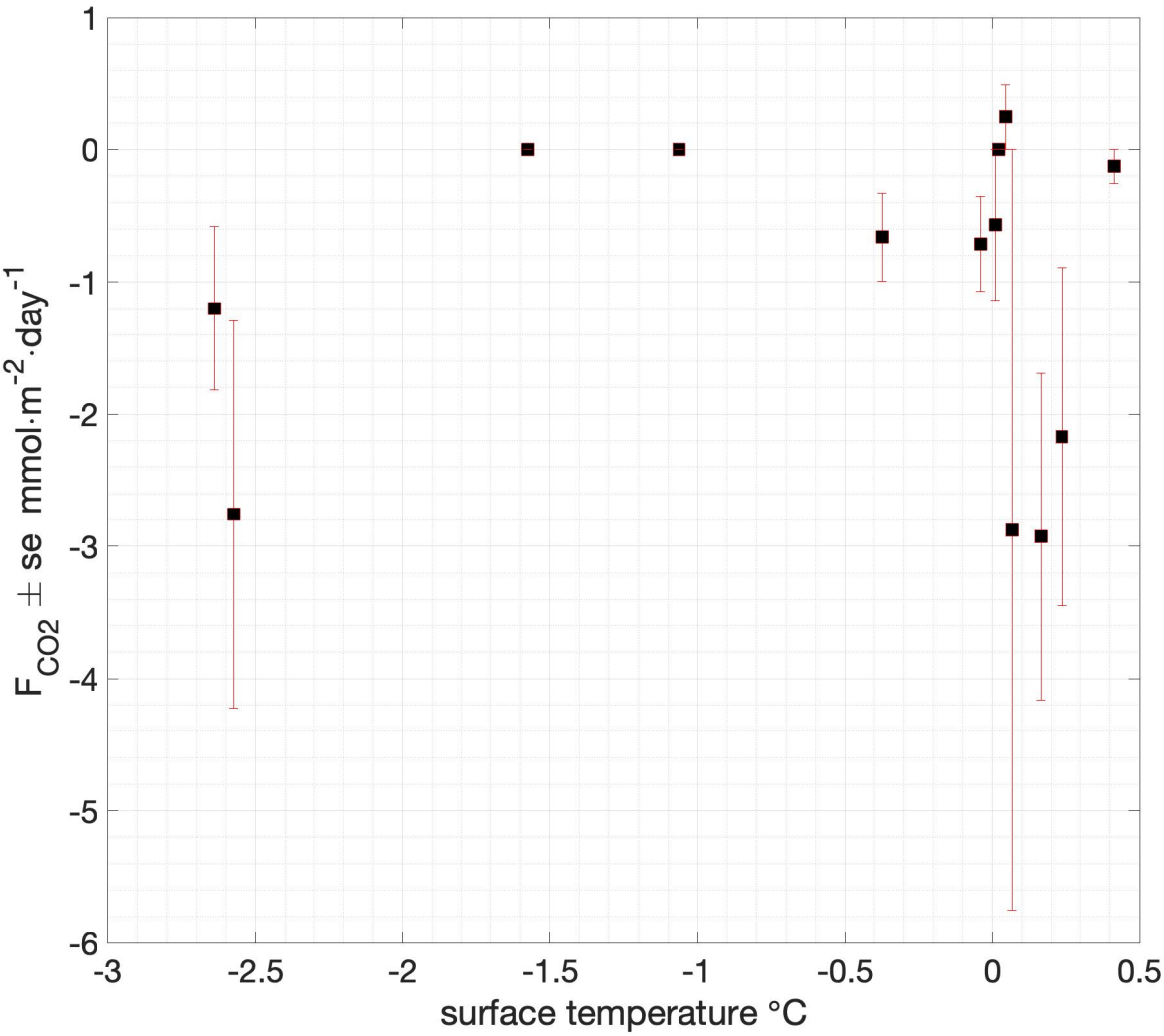

Figure 8. Surface temperature dependence of ice-air and snow-air CO_2 fluxes measured with the EGM-4 chamber flux system.

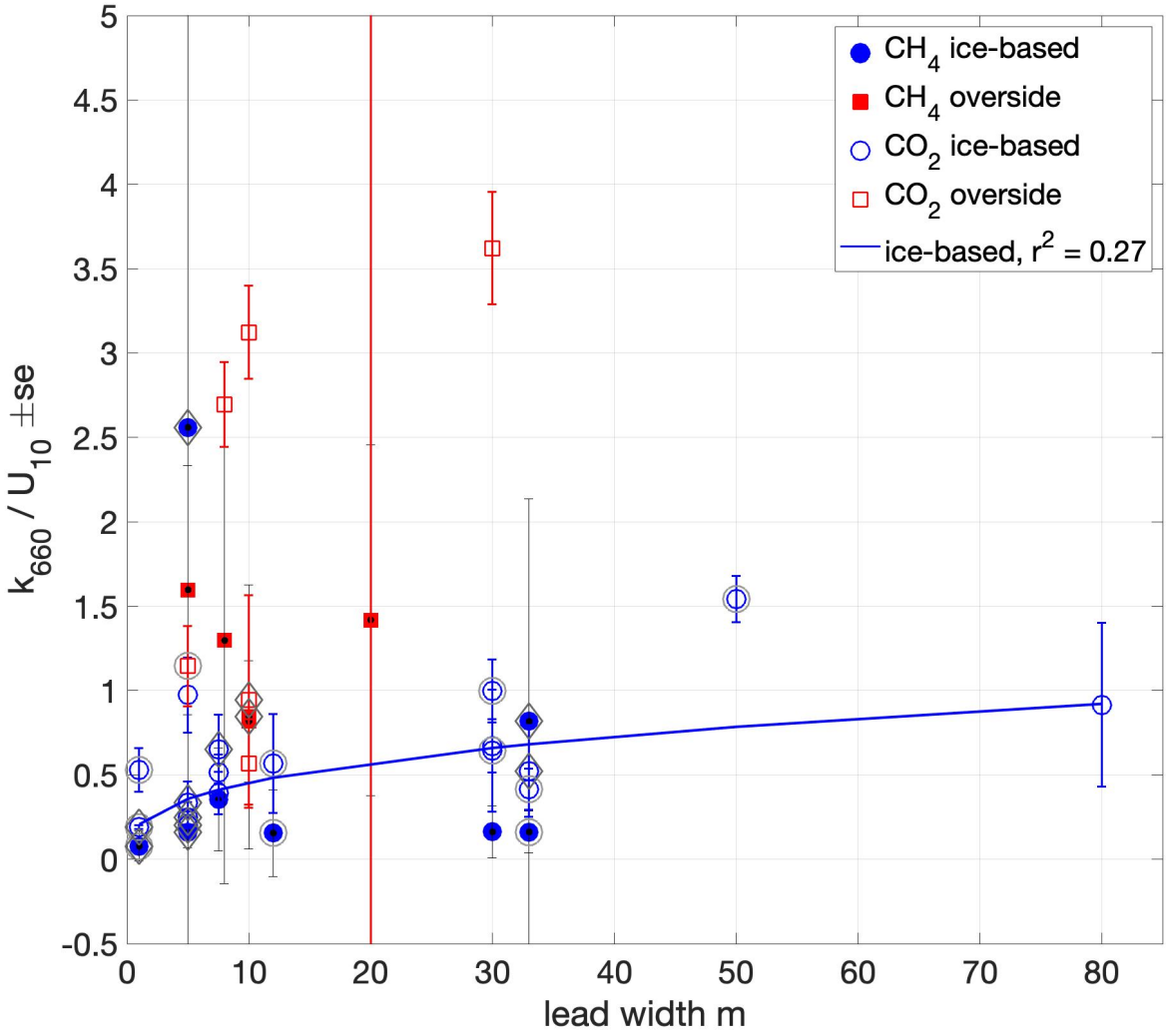

Figure 9. Dependence on lead width of water-air chamber flux-derived k_{660} normalised by U_{10}. A non-linear least squares fit to the ice-based measurements ($y = a \times x^b$) is shown (blue line). Outer circles around the markers indicate measurements made in the presence of grease ice. Diamonds indicate measurements made when surface buoyancy flux was negative (surface cooling).

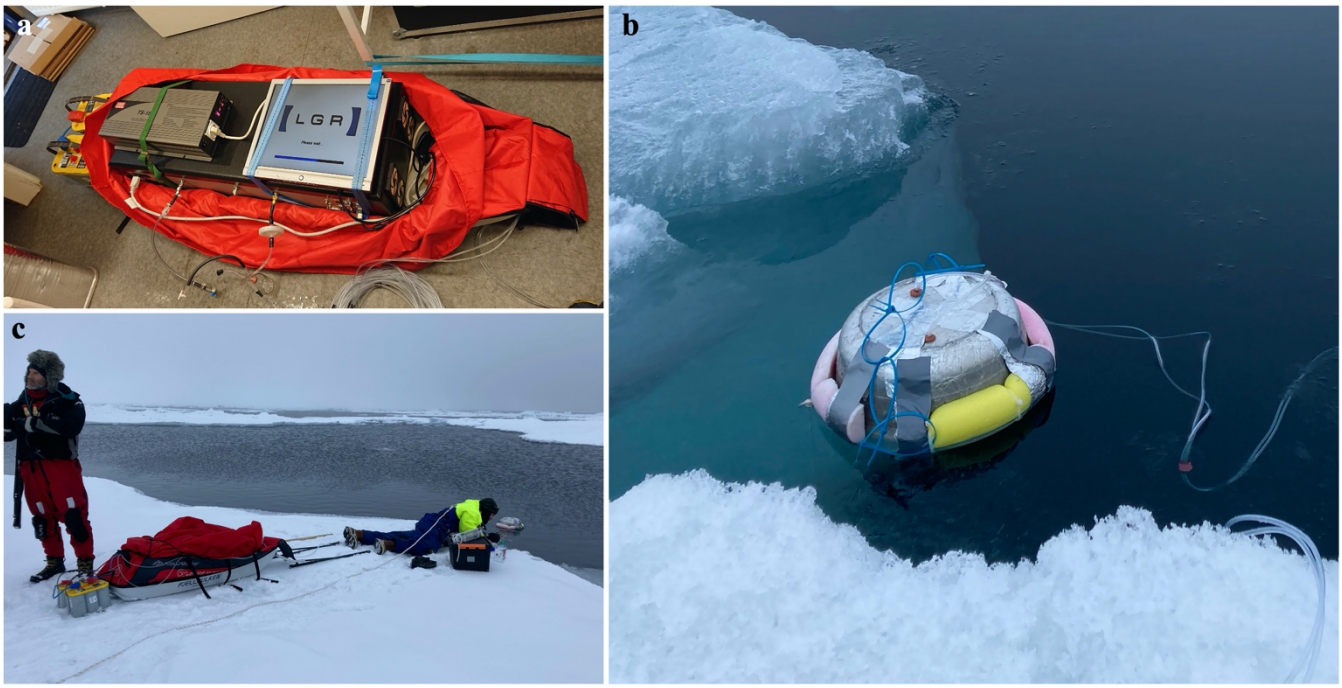

Figure S1. a) Chamber flux system consisting of an LGR Greenhouse Gas Analyser cavity enhanced laser spectrometer, power supply and tubing connections, mounted in a sled. b) Floating chamber during deployment in a sea-ice lead. c) Chamber flux system during ice-based deployment.

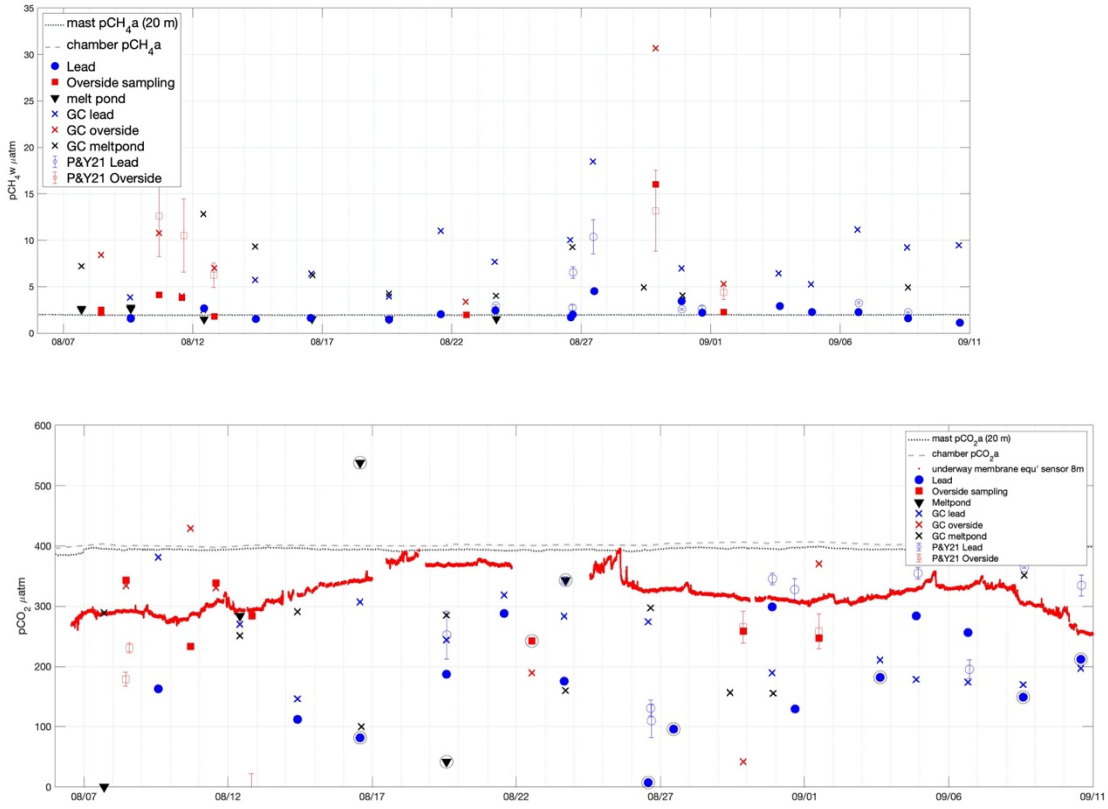

Figure S2. Time series of partial pressures of a) CH_4 and b) CO_2 in near-surface atmosphere and water during SAS2021. Solid markers show dissolved partial pressures determined from surface samples; outline markers show partial pressures determined using Eq. (1) and the parameterisation of Prytherch and Yelland (2021), excluding

unphysical negative partial pressures. Colours indicate the location from which the sample was taken. 'GC' measurements, shown as crosses, refer to the syringe-based measurements.